


Resonant Raman scattering in UO_2 revisited

Tsachi Livneh ^{*}

Department of Physics, Nuclear Research Center, Negev, P.O. Box 9001, Beer-Sheva 84190, Israel

 (Received 16 April 2021; revised 18 October 2021; accepted 9 December 2021; published 11 January 2022)

Due to UO_2 being a strong electron-phonon interaction system, resonant Raman scattering is particularly helpful in exploring the relationship between its optical properties and electronic structure. Fröhlich interaction induced resonant $2\text{LO}(\Gamma)$ phonon Raman scattering exhibits excitation energy ($E_i = 1.58\text{--}3.06\text{ eV}$), temperature ($77\text{--}873\text{ K}$), and pressure ($\leq 29\text{ GPa}$) dependent weighted contributions of two resonances. The first (incoming) resonance occurs when the incident photon energy equals the energy of an optical transition positioned at $\delta \sim 0.19$ above the $\sim 2.1\text{ eV}$ band gap. The second (outgoing) resonance occurs when the scattered-photon energy is equal to that of the optical transition. The energy of this transition is proposedly related to the Brillouin zone Γ point electronic density of states, positioned to be slightly above the band gap, by recent density functional theory calculations. The interplay between the simultaneous temperature dependent effects of tuning the band gap and altering the lifetime broadening of the excited electronic state is elucidated and demonstrated to strongly depend on the excitation energy and its position with respect to the band gap. The core difference between pressure and temperature dependent Raman response is mostly attributed to the “resonant-suppressing” role played by excited-state lifetime shortening, which becomes increasingly dominant at increased temperatures.

DOI: [10.1103/PhysRevB.105.045115](https://doi.org/10.1103/PhysRevB.105.045115)

I. INTRODUCTION

Because of its important role as nuclear fuel, the optical [1,2] and electronic [3] properties of uranium dioxide (UO_2) have been extensively studied for several decades. The electronic structure of UO_2 is largely determined by the strong correlation effects of the uranium $5f$ electrons. The large on-site Coulomb repulsion of $\sim 3\text{ eV}$ splits the $5f$ band into lower and upper Hubbard bands (LHB and UHB) [4] which form a Mott gap [3,4]. A narrow LHB band contains two well-localized $U\ 5f$ electrons and lies just below the Fermi level [3] and the levels at the onset of the UHB conduction band are composed of unoccupied f states (weakly hybridized with $O\ 2p$ orbitals). Hence, the $2.1 \pm 0.1\text{ eV}$ [1] optical band gap, E_g , is formed by $5f \rightarrow 5f$ transitions [3,5].

UO_2 crystallizes in a fluorite-type structure (space group O_h^5), where the uranium U^{+4} ions occupy the fcc sites and the oxygen O^{-2} ions occupy the tetrahedral sites. Three phonons are detected around the center of the Brillouin zone with frequencies at 278 , 578 , and 445 cm^{-1} [1,2]. They are attributed to the doubly degenerate F_{1u} IR-active transverse optical (TO) mode, nondegenerate F_{1u} IR-active longitudinal optical (LO) mode, and triply degenerate F_{2g} Raman active mode, respectively.

Gilbertson *et al.* [4] studied ultrafast dynamics of correlated electrons in UO_2 by means of femtosecond (fs) pump-probe spectroscopy. Two mechanisms were proposed to strongly affect the optical response in UO_2 upon low-energy excitations across the Mott gap, which form U^{3+} and U^{5+} among a “sea” of unexcited U^{4+} sites [4]. Both may

also involve resonant multi- $\text{LO}(\Gamma)$ -phonon Raman scattering. The first is the presence of electronic defect states in imperfect crystals that gives rise to phonon-assisted hopping (polaron conduction), leading to the formation of small polarons through the electron- $\text{LO}(\Gamma)$ -phonon interaction. In the second, the well-localized, narrow-bandwidth nature of the $5f$ electronic states suggests that these U^{3+} - U^{5+} excitations may remain localized on $5f$ sites, causing restriction of the electron mobility to form a stable exciton, predicted to have a long lifetime [4].

In a previous study we investigated the effect on the resonant Raman scattering of excitation energy E_i in the range of $1.16\text{--}2.41\text{ eV}$ and of tuning the UO_2 band gap by high pressure up to 29 GPa [6]. At ambient conditions up to sixth order multi- $\text{LO}(\Gamma)$ -phonon bands were detected with the $2\text{LO}(\Gamma)$ resonant profile being demonstrated to follow the UO_2 absorption threshold. The resonance profile of this band led to its attribution to the forbidden Fröhlich $\text{LO}(\Gamma)$ scattering, rather than to the formerly attributed [2] $\Gamma_5\text{--}\Gamma_3$ electronic Raman crystal field (CF) transition [7]. Pressure-induced redshift tuning of the band gap energy, which has been mostly attributed to the descending of the UHB unoccupied $5f$ states by compression [8], also resulted in resonant Raman scattering enhancement of the 1 and $2\text{LO}(\Gamma)$ intensities. Furthermore, resonant enhancement was not only demonstrated for E_i of 1.96 eV in proximity to E_g , but also for E_i of 1.58 eV , far below the ambient pressures E_g [6]. However, no fundamental analysis has been conducted to model the resonant dependence at those two E_i 's.

The temperature-induced resonance effect is also expected for excitation energies near the band gap and has not yet been explored; Band gap temperature tuning stems from altering the ensemble-averaged square of the phonon

*T.Livneh@nrcn.gov.il

displacement, which results from modifying the phonon population (decreasing the vibration amplitude with the decrease in temperature, which blueshifts the band gap). However, other than shifting the band gap, lowering the temperatures in excited intermediated electronic states and excitonic systems leads to an increase of the lifetime and therefore may lead to the increase in resonant enhancement [9]. In that sense, the interplay between the two contributions depends upon the departure of E_i from E_g .

The combined effect of excitation energy and temperature on the resonant Raman scattering was explored by Merlin *et al.* [10] on divalent rare-earth monochalcogenide YbS, while revealing multi-LO(Γ) resonant Raman up to the sixth order. In that system, the localized $4f^{14}$ band falls in the gap between the valence and conduction bands. The maximum in the resonance was found well above (~ 0.7 eV) the 1.4 eV band gap and it was attributed to the $4f^{13}$ hole interacting with the $5d^1$ electron within the continuum forming an f - d exciton [10,11], in spite of its forbidden symmetry. The symmetry breakdown was attributed to the spatial dispersion of the scattering tensor, which relies on the coupling of the electronic states and the LO(Γ) phonons through the Fröhlich interaction [10]. Nevertheless, the resonant effect becomes stronger upon lowering the temperatures, which was proposed to be mostly related to the decrease in the calculated lifetime broadening of the excited electronic state (from 0.1 eV at 300 K to 0.05 eV at 77 K).

The experimental results [10] were successfully analyzed by employing the solid-state analog of the configuration coordinate model. In this model it is assumed that the phonon wave functions in the excited electronic state are obtained from those of the ground electronic state by displacing the phonon coordinate by an amount which is a key parameter in the model. This mechanism is the basis of the Franck-Condon principle in molecular spectroscopy and the Raman scattering cross section for an n -phonons process is basically given by [10]

$$|R^n(\omega)|^2 = \mu^4 \left| \sum_{m=0}^{\infty} \frac{\langle n|m\rangle \langle m|0\rangle}{E_a + n\hbar\omega_{LO} - E_i + i\Gamma_a} \right|^2, \quad (1)$$

where μ is the electronic transition dipole moment, ω_{LO} is the LO(Γ) phonon energy, E_i is the incident photon energy, m and n denote the intermediate vibration level in the excited state and the final vibrational state, E_a is the electronic transition energy, and Γ_a is the linewidth of the electronic state. The Franck-Condon overlap integral $\langle n|m\rangle$ between the ground and excited states can be shown to depend on the dimensionless displacement for the Fröhlich interaction [10].

This study comprises three consecutive stages: First, we explore the ambient conditions 2LO(Γ) resonant Raman profile in an extended (up to 3.06 eV) excitation energy range. Our remarkable finding of a decrease in the normalized intensity beyond ~ 2.4 eV motivated the second stage of the study of measuring the temperature dependence at E_i below, in proximity to, and above the band gap and elucidating the interplay between the two above-mentioned simultaneous phenomena which regulate the resonant Raman cross section. Encouraged by the validation of the physical approach we engaged in reinterpretation of the source of the previously measured [6]

pressure dependent 2LO(Γ) resonant profiles at E_i below and in proximity to the ambient conditions band gap. The ability to jointly analyze the three branches of this study under a single framework is a demonstration of the invaluable usage of Raman scattering in exploring the relationship between its optical properties and electronic structure in UO₂.

II. EXPERIMENT

Raman spectra were collected in the backscattering configuration with two separate Horiba LabRAM Evolution micro-Raman spectrometers, using an excitation He-Ne laser of energy (wavelength) 1.96 eV (632.8 nm); diode lasers of energies 1.58 eV (785 nm), 2.33 eV (532 nm), and 3.06 eV (405 nm); and a Horiba LabRAM HR 800 spectrometer using Ar ion lasers of 2.41 eV (514.5 nm) and 2.54 eV (488 nm). Temperature dependent spectra were measured by means of a Linkam continuously cooled liquid-nitrogen unit with a THMS600 stage plate. The UO₂ sample was synthesized by sintering of UO₂ powder in hydrogen flow at 1700 °C [6]. The pellet is constructed from ~ 20 μ m single crystals with various (unidentified) crystallographic orientations. Polishing of the pellet was followed by x-ray diffraction (XRD) measurements in order to verify the very good structural quality of the sample using a Bruker D8 diffractometer in a Bragg-Brentano configuration (Cu $K\alpha$ source); see Fig. S1 of the Supplemental Material [12] (see, also, Refs. [13–24] therein).

III. RESULTS AND DISCUSSIONS

A. Raman scattering symmetry assignments revisited

Figure 1 shows the low temperature (77 K) Raman spectrum of UO₂ in the range of 180–2600 cm^{-1} , measured at the excitation energy of 2.33 eV with a Lorentzian line-fit analysis, from which the central positions of the various bands are denoted. Table I summarizes the lower spectral range bands (up to ~ 1230 cm^{-1}) with their proposed assignments. The frequencies of the Brillouin zone edge phonons were extracted from the recently measured phonon dispersion curves of UO₂ [14], which updated those of a former study [15].

Recent studies explore polarized first-order Raman scattering of the F_{2g} mode at various well-defined crystallographic planes within a single crystal [20] or particular grains within a polycrystalline pellet of UO₂ [25]. A full symmetry analysis of the contributing scattering tensors at the Γ point for the second-order transitions is presented in Sec. 2 of the Supplemental Material [12] and may facilitate the extension of polarized Raman studies beyond the first order.

In the low spectral range (inset of Fig. 1) a broad peak at ~ 290 cm^{-1} consists of four bands which are assigned to second-order bands of Brillouin zone edge acoustic phonons. We assign the ~ 238 cm^{-1} band to $2TA(L)$, the 290 cm^{-1} band to $LA(L)+TA(L)$, the band at ~ 364 cm^{-1} to $LO_R(L)+LA(L)$, and the weak band at ~ 415 cm^{-1} to $2LA(X)$. The 77 K F_{2g} symmetry Raman-allowed mode [$R(\Gamma)$] is found in ~ 447 cm^{-1} . At a higher part of the spectrum, we find in addition to this band, a broad band that contains three distinguishable contributions centered at ~ 552 , ~ 584 , and ~ 627 cm^{-1} . The former is attributed to the second order of the

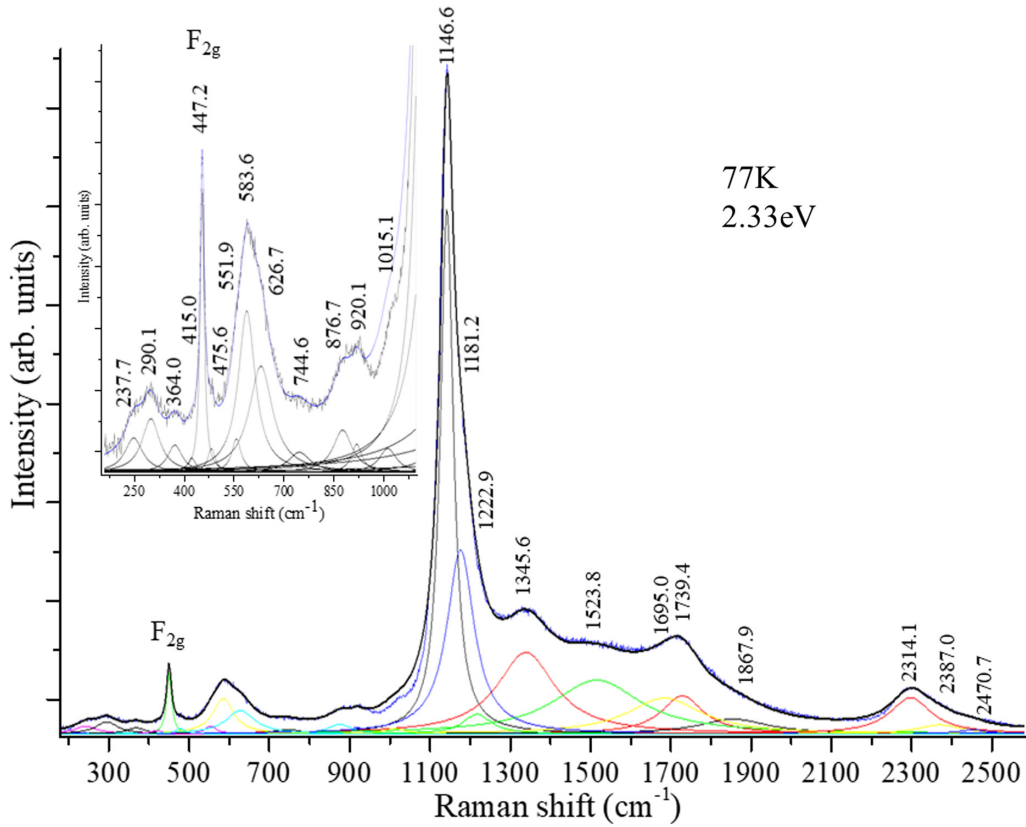


FIG. 1. Raman spectrum of UO_2 in the range of 180–2600 cm^{-1} , measured at 77 K and excitation energy of 2.33 eV with the denoted spectral positions. In the inset, the enlarged view of the lower spectral range is shown.

Brillouin zone center TO phonons, $2\text{TO}(\Gamma)$, the second to the Raman-forbidden $\text{LO}(\Gamma)$ phonon, which appears under resonant conditions [6] and the latter band is not attributed to UO_2 (as suggested in Ref. [6]) but rather to surface-formed U_4O_9 [26] impurities. It is important to note that under off-resonant conditions, where the $\text{LO}(\Gamma)$ intensity is strongly reduced (and therefore practically absent from the 1.58 eV spectrum) [6], the low temperature $2\text{TO}(\Gamma)$ band is strongly manifested. A strong band at 1147 cm^{-1} is attributed to $2\text{LO}(\Gamma)$ [6]. At slightly higher energy a shoulder to the $2\text{LO}(\Gamma)$ at ~ 1181 cm^{-1} , which is particularly dominant away from resonance (not being overshadowed by the former), is assigned to $2\text{LO}(\text{L})$. Due to its significant contribution, its intensity has

TABLE I. Proposed assignments for the lower spectral range of UO_2 Raman scattering at 77 K.

ν (cm^{-1})	Assignment	ν (cm^{-1})	Assignment
238	$2\text{TA}(\text{L})$	627	U_4O_9 (at the surface)
290	$\text{LA}(\text{L}) + \text{TA}(\text{L})$	745	$2\text{TO}_\text{R}(\text{L})$
364	$\text{LO}_\text{R}(\text{L}) + \text{LA}(\text{L})$	877	U_4O_9 (at the surface)?
415	$2\text{LA}(\text{X})$	920	$2\text{TO}_\text{R}(\text{X})$
447	$\text{R}(\Gamma)$	1015	?
476	$\text{TO}_\text{R}(\text{L}) + \text{TA}(\text{L})$	1147	$2\text{LO}(\Gamma)$
552	$2\text{TO}(\Gamma)$	1181	$2\text{LO}(\text{L})$
584	$\text{LO}(\Gamma)$	1223	$2\text{LO}(\text{X})$

to be taken into account in analyzing the resonant $2\text{LO}(\Gamma)$ intensity profile. At ambient pressures and temperatures up to sixth-order polarized multi- $\text{LO}(\Gamma)$ -phonon bands are detected and attributed to “forbidden” Fröhlich LO scattering [6]. Under this framework the bands at 1739 and 2314 cm^{-1} are attributed to $3\text{LO}(\Gamma)$ and $4\text{LO}(\Gamma)$, respectively. A high temperature shoulder to the latter contains two broad bands with unclear origin, which might be suggested to stem from off-Brillouin zone edge acoustic phonon sidebands [27].

We turn now to the middle spectral range. Inelastic neutron scattering (INS) measurements reveal intramultiplate crystal-field (CF) transitions within the ground electronic state (with predominant 3H_4 character). The ground state is of Γ_5 symmetry triplet, followed by a Γ_3 doublet, a Γ_4 triplet, and a Γ_1 singlet [28,29]. In that sequence the $\Gamma_5 \rightarrow \Gamma_3$ INS transition is found at ~ 150 meV, $\Gamma_5 \rightarrow \Gamma_4$ at ~ 166 meV, and $\Gamma_5 \rightarrow \Gamma_1$ at ~ 175 meV, i.e., at 1210, 1339, and 1411 cm^{-1} , respectively. From a series of bands that are distinguishable in Fig. 1, the 1223 cm^{-1} can be assigned to $\Gamma_5 \rightarrow \Gamma_3$ or to $2\text{LO}(\text{X})$ and the 1345 cm^{-1} can potentially be assigned to $\Gamma_5 \rightarrow \Gamma_4$, but the three bands at 1523, 1695, and 1868 cm^{-1} are not straightforwardly assignable; despite the decreased intensity with temperature (see below), which points to their origin of electronic Raman scattering [7] (since at equilibrium, the population of the CF levels obeys the Boltzmann statistics [30]), their energy is higher than those of the ground-state intramultiplate crystal-field transitions. In addition, their energy

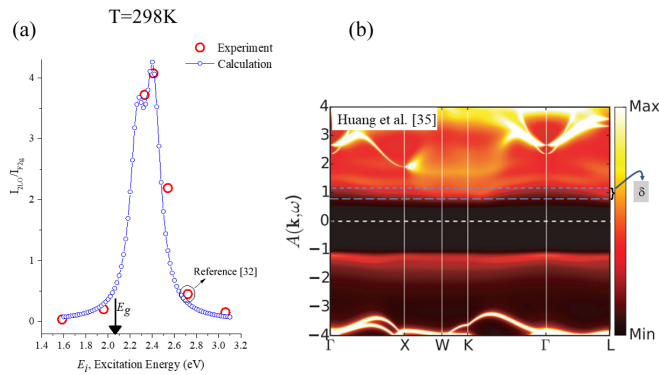


FIG. 2. (a) The intensity of ratio $R[2\text{LO}(\Gamma)/F_{2g}]$ as a function of E_i , extracted from Lorentzian line-fit analysis with a calculated fit which is discussed in Sec III C. (b) The momentum-resolved spectral function $A(k, \omega)$ obtained by the DFT + DMFT method. Reproduced with permission from Huang *et al.* [35].

being higher than the highest possible second-order phononic features [14,15] argues against their pure phononic nature. A scenario that cannot be ruled out for a system with close proximity of CF and phononic states (possibly higher than first order) is the formation of mixed electronic-phononic states [31]. Further studies and extensive scrutiny are needed for resolving this issue.

B. Excitation energy dependent $2\text{LO}(\Gamma)$ resonant Raman under ambient conditions

In what follows we extend the qualitative discussion on the resonant Raman profile under ambient conditions, previously presented within an excitation energy range limited to 2.41 eV [6]. Figure S2 in the Supplemental Material [12] presents the Raman spectra of UO_2 at excitation energies E_i in the range of 1.58–3.06 eV after the intensity of the most prominent $2\text{LO}(\Gamma)$ band is calibrated and normalized to that of the F_{2g} mode. For clarity, close comparison between the spectra measured at 2.33 and 2.41 eV is also shown in Fig. S3 [12].

Figure 2(a) shows with red empty circles the E_i dependent intensity ratio $R[2\text{LO}(\Gamma)/F_{2g}]$, extracted from a Lorentzian line-fit analysis. We take the Raman cross section of the F_{2g} mode to be independent of the excitation energy (and in the forthcoming analysis also independent of pressure and temperature). The extracted R ratio for 2.72 eV [32] is added to Fig. 2(a). Remarkably, resonant Raman scattering of the $2\text{LO}(\Gamma)$ band is found within a narrow “stripe” [with a full width at half maximum (FWHM) of ~ 0.35 eV] of low-lying $5f$ states, peaked at ~ 0.35 eV above the band gap.

Unlike for YbS [10], where the excitation was attributed to a particular (excitonic) state positioned ~ 0.7 eV above the band gap, for UO_2 we are unable, based on our current knowledge, to uniquely single out a designated state above the band gap. Nevertheless, since contributions to the Raman susceptibility are not necessarily equivalent for all the Brillouin zone critical points [33,34] the resonant Raman excitation profile may be peaked at higher energies than the optical band gap. In order to explore the possible attribution of a selective resonant excitation we look into the momentum-resolved spectral function $A(k, \omega)$, calculated by Huang *et al.* [35] by the density

functional theory plus single-site dynamical mean field theory (DFT+DMFT) method; Fig. 2(b) is adapted from Ref. [35]. The spectral function provides information about the nature of the allowed electronic states, and can be considered as a generalized density of states (DOS). The DOS peak at the Γ point is shown to be higher (denoted by an extent of δ) above the energies of the X, W, K, and L points of the Brillouin zone, which corresponds to the band gap energy. Hence, the resonant Raman is argued to be peaked near the Γ point of the Brillouin zone with an energy slightly higher than the band gap energy of ~ 2.1 eV [1]. Our working hypothesis considers a dominant role played by optical excitation around the Γ point maximal DOS, which leads to Fröhlich interaction induced resonant Raman scattering of the $\text{LO}(\Gamma)$ mode and its overtones and we shall generally refer henceforward to this state as the “excited electronic state” or “intermediate state” [36]. We note the very good correspondence between experimental E_i dependent R ratios and the calculated fit represented by the blue dotted line in Fig. 2(a). For clarity of representation, we delay to Sec. III C the elaborated discussion on the approach taken to provide this fit.

C. Temperature dependent $2\text{LO}(\Gamma)$ resonant Raman in the range of 77–873 K

Figures 3(a)–3(c) show the temperature dependent Raman spectra of UO_2 in the 150 – 2900 cm^{-1} range for E_i of 2.33 eV (a), 1.96 eV (b), and 1.58 eV (c), which represent the cases of $E_i > E_g$, $E_i \approx E_g$, and $E_i \ll E_g$, respectively. It is clear that only in the former case the $\text{LO}(\Gamma)$ up to its fourth-order shows a distinct resonant enhancement upon decreasing temperatures.

Figure 4 presents the experimental R ratios after both $2\text{LO}(\Gamma)$ and F_{2g} intensities being divided by the temperature dependent Bose-Einstein phonon occupation factors of the Stokes scattering, i.e., $[n(\omega_{\text{LO}}) + 1]^2$ and $[n(\omega_{F_{2g}}) + 1]$, respectively (with the phonon distribution at the ω_{ph} frequency being $n(\omega_{ph}) = [\exp(\omega_{ph}/kT) - 1]^{-1}$ [34]). In addition, the R ratios at 1.96 eV from room temperature up to 873 K (depicted in red crossed empty squares) are extracted from a study by Elorrieta *et al.* [24] that explored the high temperature range, which is also in agreement with the results of the study by Guimbretière *et al.* [37]. For clarity of representation the approach taken to model and fit the temperature dependent R ratios at the three measured E_i 's is delayed to three paragraphs below.

Elucidating the nature of the resonant Raman scheme requires a well-defined temperature dependence of the band gap and a reliable assessment of the temperature dependent broadening parameter. We first evaluate the temperature dependence of the band gap, assisted by the extracted data (Fig. S4 [12] adapted from the study of Griffith and Hubbard [21]) for the UO_2 sample at the temperature range of 85–985 K with the extrapolation to a low absorptivity. The band gap at 85 K is of 2.13 eV and decreases to 2.07 eV at room temperature, which is consistent with the well-accepted result of 2.1 ± 0.1 eV [1]. Aided by the five extrapolated energies we calculate the temperature dependence, while employing the methodologic approach of Ruello *et al.* [22]. The calculated temperature dependence of the optical absorption edge in UO_2 (and therefore the band gap), shown

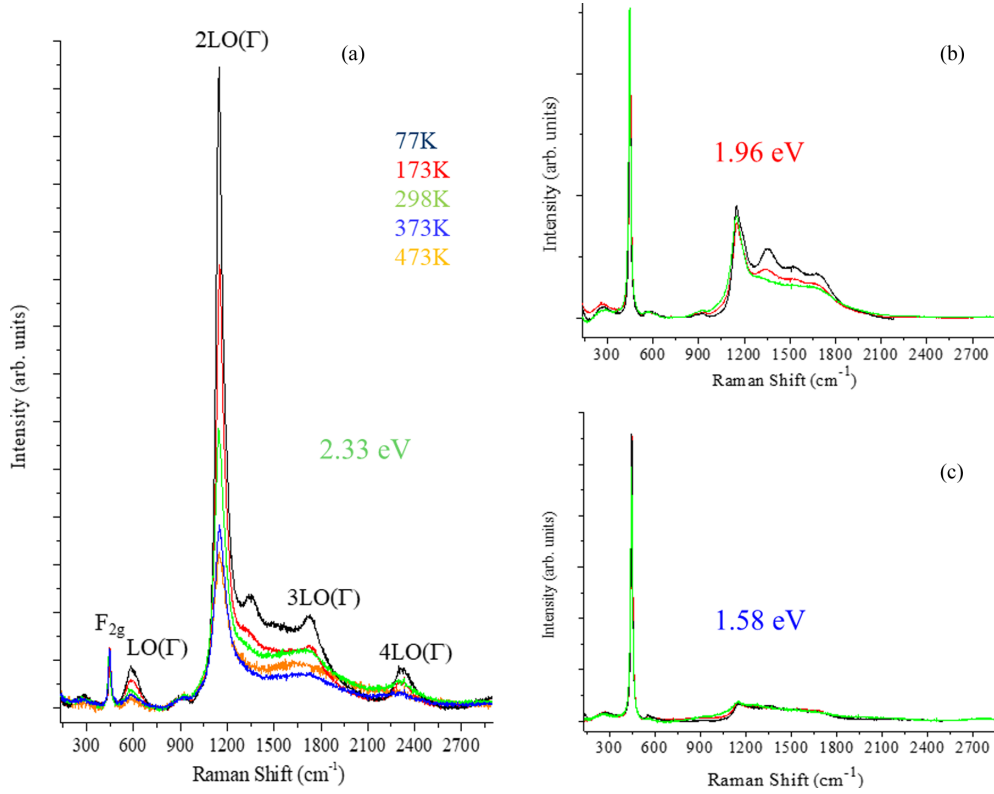


FIG. 3. Temperature dependent Raman spectra of UO_2 , measured at the excitation energies of 2.33 eV (77–473 K) (a), 1.96 eV (77–298 K) (b), and 1.58 eV (77–298 K) (c). Spectra are normalized by the intensity of the F_{2g} Raman-allowed mode.

in Fig. 5(a) with empty black circles, can be described as $E_g(T) = E_g^0 + \beta[n(\omega_{\text{LO}}) + 1]$ with $E_g^0 = 2.81$ eV, $\beta = 0.69$, and the Bose-Einstein distribution of the $\text{LO}(\Gamma)$ phonon $n(\omega_{\text{LO}})$, at 578 cm^{-1} [1]. The calculated dependence (solid black line) adequately follows the experimental estimates and one can roughly extract between 300 and 1000 K a temperature coefficient of $(\frac{\partial E_g}{\partial T}) = 6 \times 10^{-4}$ eV.

In a following step we evaluate the temperature dependence of the broadening parameter; for a transition in semiconductors, it is described by [38]

$$\Gamma_a(T) = \Gamma_0 + \frac{\Gamma_{\text{LO}}}{e^{(\Theta_{\text{LO}}/T)} - 1}. \quad (2)$$

Above, the width Γ_0 originates from temperature independent mechanisms. Γ_{LO} is a measure of the strength of electron (exciton)–LO phonon interactions, while Θ_{LO} is the LO phonon temperature. We reasonably fit Γ_0 to be 0.05 eV and set Θ_{LO} to be 830 K. The most significant challenge in solving Eq. (2) is deducing the value of Γ_{LO} . In Fig. S5 we fit the experimental results for E_i of 1.96 eV (Fig. 4) with a set of Γ_{LO} that span from 0.2 to 0.48 eV [12]. We clearly observe the effect of the lifetime broadening of the intermediate state on the “flattening” of the temperature dependence at the higher temperatures. The best correlation to the experimental data is achieved for Γ_{LO} of 0.46 eV.

Following a proposed scenario, which positions the energy of the resonant state at $\delta \sim 0.19$ eV beyond the band gap, and while considering δ to be temperature independent, we present (blue line) in Fig. 5(a) the temperature dependence

of $E_g(T) + \delta$. For considering the case [10], for which the resonance of the first overtone is expected at $2\hbar\omega_{\text{LO}}$ beyond the resonant state [Eq. (1)], we also present the temperature dependence of $E_g(T) + \delta + 2\hbar\omega_{\text{LO}}$ (orange line). The temperatures at which two of the three measured E_i 's intercept $E_g(T) + \delta$ and $E_g(T) + \delta + 2\hbar\omega_{\text{LO}}$ are extracted by depicting horizontal dashed lines that represent the energies of the measured E_i 's. The interceptions of 2.33 eV (green) and 1.96 eV (red) with those two curves are marked with gray circles as 1 and 2 (~ 80 – 120 and ~ 450 K) and 3 and 4 (~ 780 and ~ 970 K), respectively.

In order to fit the temperature dependence of the R ratio, shown in Fig. 4, we assume the activity of two resonances denoted as I_{out} and I_{in} .

$$I_{\text{out}} \sim \left| \frac{C_2}{E_a - E_i + 2\hbar\omega_{\text{LO}} + i\Gamma_a} \right|^2 \quad (3)$$

is actually a “reduced” form of Eq. (1) [10], which considers only a single intermediate vibration level in an excited state E_a for the first $\text{LO}(\Gamma)$ overtone and occurs when the scattered-photon energy is equal to that of the optical transition in the lattice. The second contribution,

$$I_{\text{in}} \sim \left| \frac{C_1}{E_a - E_i + i\Gamma_a} \right|^2, \quad (4)$$

occurs when the incident photon energy equals the energy of the optical transition and represents the resonance with the state positioned at δ beyond the band gap, i.e., $E_a \approx E_g + \delta$. C_1 and C_2 are adjustable parameters, which do not

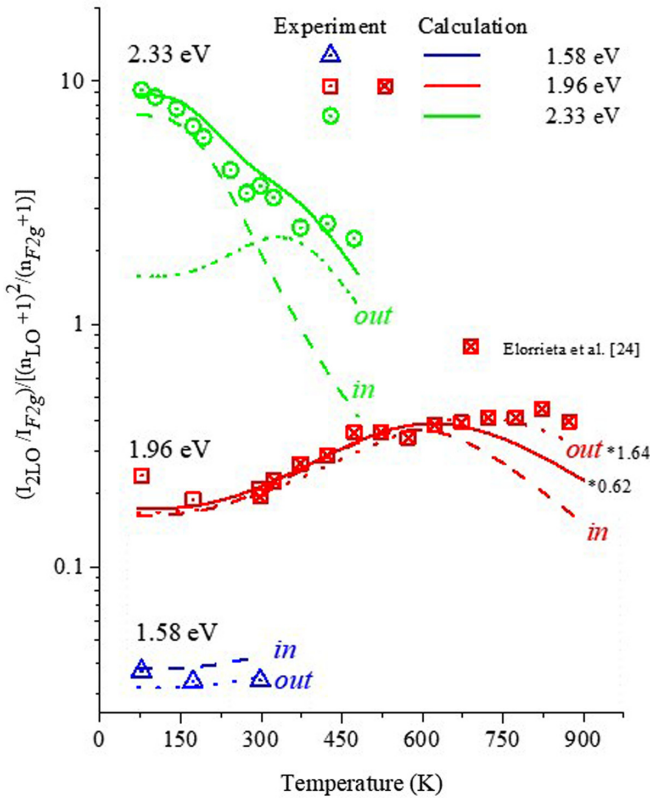


FIG. 4. (a) The experimental and calculated dependence of the R ratio on temperature (normalized by Bose-Einstein phonon population distributions) for the denoted E_i 's. The R ratios at 1.96 eV from room temperature up to 873 K are extracted from Elorrieta *et al.* [24]. The calculated fits for I_{in} , I_{out} and $I_{in} + I_{out}$ are shown with dashed, dotted, and solid lines, respectively; see text. The parameters used in the calculations are summarized in Table S4 [12]).

differ significantly in their values within the calculated fits (Table S4 [12]).

The points of interceptions, marked with gray circles in Fig. 5(a), do not take into account the finite lifetime of the electronic state, as manifested in Eqs. (3) and (4) by the broadening parameter Γ_a . Hence, we present in Figs. S6(a) and S6(b) for E_i of 2.33 and 1.96 eV, respectively, the temperature dependence of the denominator (squared) for I_{in} and I_{out} for various Γ_a 's. Although $\Gamma_a = 0.46$ eV is the value employed in the calculations, we present a series of three Γ_a 's : 0.16 (blue), 0.46 (black), and 0.76 eV (red). The utmost importance of the adequate inclusion of the lifetime effect is clearly demonstrated. As expected, with increasing Γ_a the resonant temperature (minimum in the denominator) is shifted to low temperatures, as is indicated by the black arrows in Fig. 5(a), which relate to the $\Gamma_a = 0.46$ eV case. For example, point 2 (I_{out} at E_i of 2.33 eV) is shifted in its position by ~ 120 K toward ~ 330 K.

Figures 5(b)–5(d) show the calculated R ratio as a function of temperature up to 900 K at various E_i in the range of 1.5–3.1 eV for I_{in} , I_{out} , and $I_{in} + I_{out}$, respectively. The temperature dependent excited electronic state energy is taken to be similar to the temperature dependence of the band gap energy.

The calculated R ratios for the three E_i 's within the measured temperature ranges discussed in this study are highlighted with thick lines and are also replicated in Fig. 4, with dashed, dotted, and solid lines, respectively. In Fig. 5(d) the calculated room temperature E_i dependence of $I_{in} + I_{out}$ in the 1.5–3.1 eV range is also shown (black) and replicated in the calculated blue dotted line of Fig. 2(a) that uses the room temperature values of $E_g = 2.07$ eV and $\Gamma_a = 0.08$ eV.

The correlations in Figs. 4 and 2(a) between the calculated curves [Fig. 5(d)] and the experimental results are remarkable, considering the complexity of the electronic structure of UO_2 and the assumptions made under the approach taken [39]. Returning to Fig. 4 for the 2.33 eV low temperature results in the calculated “shift” between the dominant contribution of I_{in} to that of I_{out} , seen slightly above room temperature, being nicely reproduced in the experiment. The solid green line in Fig. 4 represents the sum of two contributions, i.e., $I_{in} + I_{out}$. For 1.96 eV some indicated minor scaling had to be introduced for clarity of representation. Up to 600 K the general dependence of the I_{in} and I_{out} profiles are practically similar. Beyond this temperature the “flatness” of the temperature dependence better matches the calculated temperature dependent profile of I_{out} with Γ_a of 0.46 eV (comparing to $I_{in} + I_{out}$). The need for scaling and the general close correspondence with I_{out} may be attributed to the fact that away from resonance and at higher temperatures more intricate effects, that are not included in the calculations, may play a role.

The fundamentally important result of this study is the resonant optical transition being positioned at $\delta \sim 0.19$ eV above the band gap energy. The correlation between optical and electronic spectroscopies is dictated by the fundamental physics of the transitions/processes involved. Optical measurements are helpful in revealing the electronic structure [1,2], but may only reveal unoccupied $6d$ states in the conduction band, because of the dipole selection rules. In contrary, bremsstrahlung isochromat spectroscopy (BIS) and x-ray absorption spectroscopy (XAS) indicated that the bottom of the conduction band is mainly composed of U $5f$ states [5], which is also confirmed by theoretical studies [3]. The proposed relation of the $2\text{LO}(\Gamma)$ resonant excitation profile to the Brillouin zone Γ point electronic DOS, which deserves a closer theoretical scrutiny, may be argued to be another example of the beneficial combination of optical and electronic spectroscopies in the exploration of the electronic structure in UO_2 .

Temperature may simultaneously affect the resonance Raman intensity by tuning the band gap and the lifetime broadening of the excited electronic state [34]. Temperature-induced lifetime effects are extensively affected by the role played by nonradiative transitions, with the temperature dependence of the mean lifetime of the excited electronic state being related to the thermal relaxation time, which scales with $\exp(E_A/kT) - E_A$ being the threshold energy required by the excited state electrons to attain the channel of nonradiative recombination [40].

The interplay between the temperature effects of band gap tuning and lifetime broadening of excited electronic state strongly depends on the excitation energy and its position with respect to the maximal R ratio. Under off-resonant conditions,

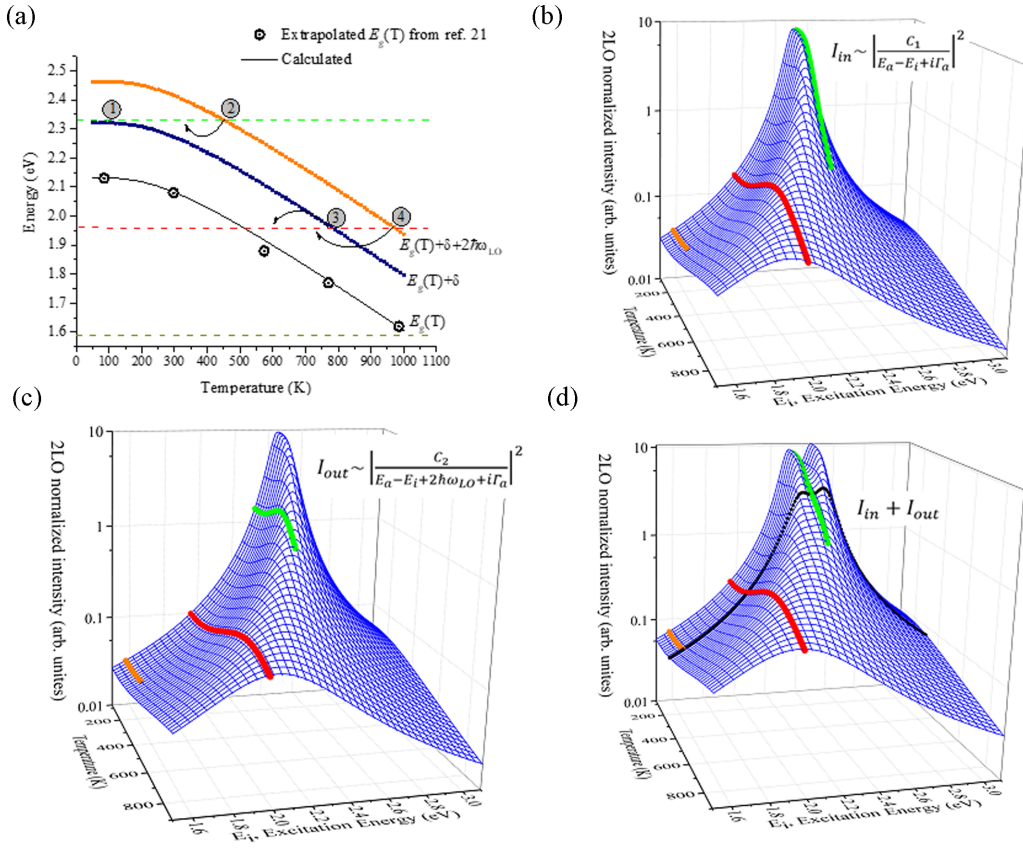


FIG. 5. (a) The extrapolated optical UO_2 absorption edge for spectra measured at the temperature range of 85–985 K (black empty circles) [21] and their calculated temperature dependence according to $E_g(T) = E_g^0 + \beta(n(\omega_{LO}) + 1)$ — see text. Blue and orange lines present the temperature dependence of $E_g(T) + \delta$ and $E_g(T) + \delta + 2\hbar\omega_{LO}$, respectively. The interceptions of 2.33 eV (green) and 1.96 eV (red) with those two curves are marked with gray circles as 1 and 2 and 3 and 4, respectively. Black arrows represent the temperature shift in the resonant R ratios by introducing broadening parameters of the $\Gamma_a = 0.46$ eV into Eqs. (3) and (4). (b) The calculated R ratio as a function of temperature up to 900 K at various E_i 's in the range of 1.5–3.1 eV for I_{in} . The calculated R ratios for the three measured E_i 's are highlighted with thick green, red, and orange lines, respectively; (c) the same for I_{out} ; (d) the same for $I_{in} + I_{out}$. The calculated room temperature E_i dependence of $I_{in} + I_{out}$ in the 1.5–3.1 eV range is also shown (black) and replicated as the calculated blue line in Fig. 2(a).

other than considering the phonon occupation effects for the $2\text{LO}(\Gamma)$ band, no significant effect of temperature is found on its intensity, as indeed is expected. For $E_i > E_g$, lowering the temperature from 300 to 77 K leads to a ~ 2.5 -fold increase in the R ratio [as well as to the intensities of $\text{LO}(\Gamma)$ and its third and fourth overtones; see Fig. 3(a)]. Nevertheless, it is difficult to exclusively relate such an extensive R ratio increase to the corresponding ~ 0.05 eV blueshift of the band gap [see $E_g(T)$ in Fig. 5(a)], and we therefore attribute the most significant contribution to the R ratio increase to decreasing the lifetime broadening of the intermediate electronic state. We are left with the most intricate case of $E_i \approx E_g$. At 77 K the excitation energy is below the band gap and therefore lifetime effects do not play a significant role. Increasing the temperature redshifts the band gap, which turns the system more resonant, but also enhances the lifetime broadening of the excited electronic state and therefore decreases the R ratio. With a band gap temperature coefficient of ~ 0.6 meV/K [21] the temperature at which the system should be resonantly peaked may reach ~ 750 K, for which shortening the lifetime of the excited electronic state will result in an opposite effect to that of resonant

tuning and will lead to a minor overall effect on the R ratio. Hence, the temperature dependence for the $E_i \approx E_g$ at 1.96 eV shows a rather weak monotonic increase in the R ratio.

D. Pressure dependent $2\text{LO}(\Gamma)$ resonant Raman up to 29 GPa

In order to elucidate the nature of resonant Raman scattering in UO_2 we revisit our previously measured pressure dependence of the $2\text{LO}(\Gamma)$ band intensity (at 300 K and up to 29 GPa) for E_i below (1.58 eV) and in proximity to (1.96 eV) the ambient conditions band gap energy [6], and present the R ratios in Fig. 6(a) with filled blue triangles and red squares, respectively. The maximal R ratio for E_i of 1.96 eV is at ~ 16 GPa, which correlates with $V/V_0 \sim 0.93$ [8], for which the calculated effect of pressure on the $5f$ states DOS was clearly demonstrated to be significant [8,35]. Furthermore, even for the 1.58 eV excitation energy, far below the ambient conditions band gap, the system turns out to be resonant at high pressures (~ 22 GPa), demonstrating that resonance Raman can also be achieved by redshifting the band gap by high pressure [6].

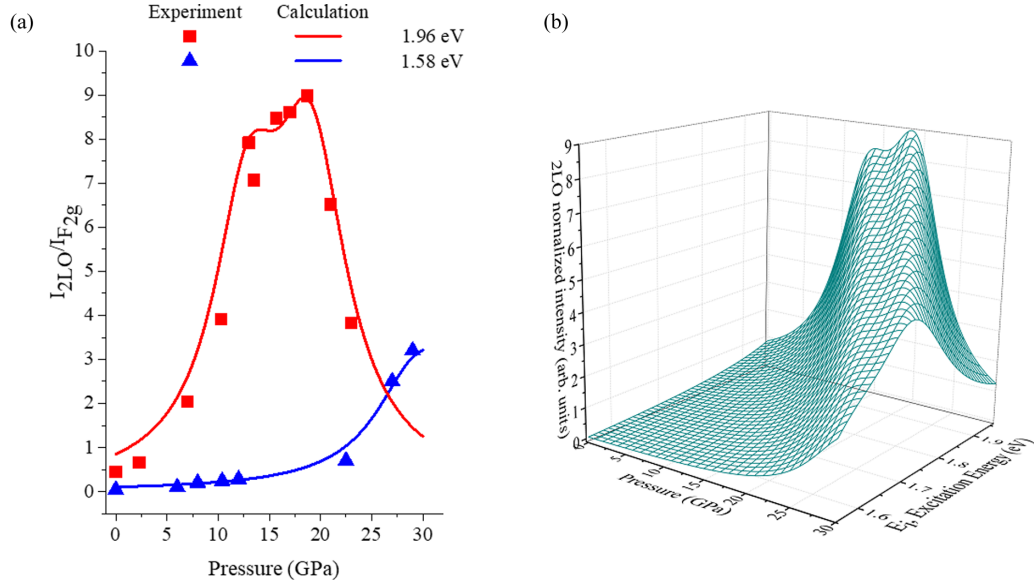


FIG. 6. (a) The experimental [6] and model-fitted dependence of the R ratio on pressure for the denoted E_i 's. (b) The calculated dependence of the 2LO(Γ) intensity on pressure for the excitation energies range of 1.55–1.96 eV. The parameters used in the calculations are summarized in Table S4 [12].

The extension of the resonant Raman profile measurements beyond 2.41 eV [6] calls for modeling the experimental results and particularly for reattributing to the physical origin of the descending R ratio found for E_i of 1.96 eV beyond ~ 16 GPa. Figure 6(b) presents the calculated pressure dependent R ratio at various E_i 's in the range of 1.55–1.96 eV by employing Eqs. (3) and (4) when $E_g(P) = E_g(0) + \alpha P$ with $E_g(0) = 2.07$ eV, $\alpha = (\frac{\partial E_g}{\partial P})_{300K} = 0.023$ eV/GPa, and $\Gamma_a(P) = (0.08 + 0.001P)$ eV, P being the pressure in GPa. Increasing the pressure shifts the maximum R ratio to lower E_i 's, but also decreases its intensity. Based on those calculated profiles, a fit of the experimental [6] pressure dependent R ratios for $E_i = 1.96$ eV (red line) and 1.58 eV (blue line) is shown in Fig. 6(a) by employing Eqs. (3) and (4) and calculating $I_{in} + I_{out}$ with weighted contribution expressed in Table S4 [12]. Considering the assumptions made, very

good agreement with experiments is obtained when using a pressure coefficient, α , that reasonably agrees with that recently reported [23]. The most important physical notion is that the decrease in the R ratio beyond ~ 16 GPa can be attributed to detuning from resonance of the Raman process while being consistent with the 2LO(Γ) resonant excitation profile in Fig. 2(a).

E. Tuning the 2LO(Γ) resonant Raman with respect to $E_i - E_g$

Figure 7 presents the calculated high pressure [Fig. 7(a)] and temperature [Fig. 7(b)] dependent R ratio on $\Delta = E_i - E_g$, by employing Eqs. (3) and (4) and calculating $I_{in} + I_{out}$ with the parameters used summarized in Table S4 [12]. For the pressure dependent case increasing E_i results in upshifting the “ Δ window,” which mostly affects the weighted contribution of I_{in} vs I_{out} , but only has a minor effect on the overall

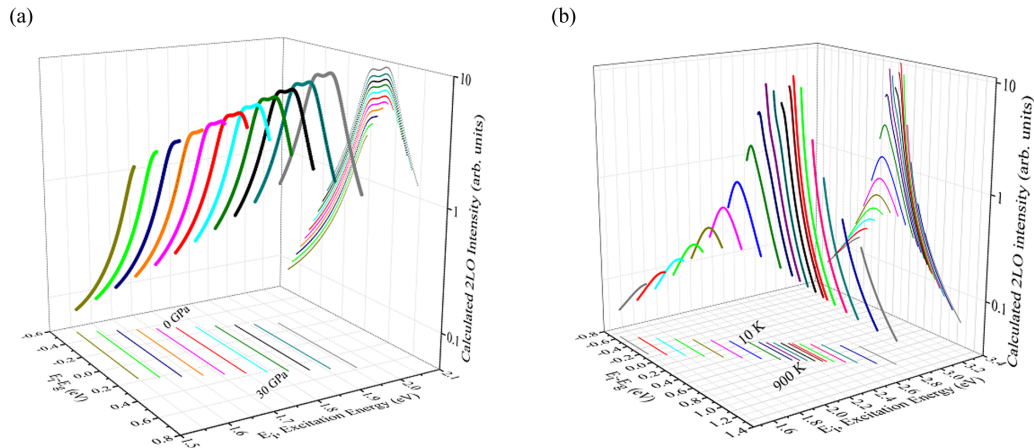


FIG. 7. (a) The calculated pressure dependent 2LO(Γ) intensity for a ramp of $\Delta(P) = E_i - E_g(P)$. (b) The calculated temperature dependent 2LO(Γ) intensity for a ramp of $\Delta(T) = E_i - E_g(T)$. The parameters used in the calculations are summarized in Table S4 [12].

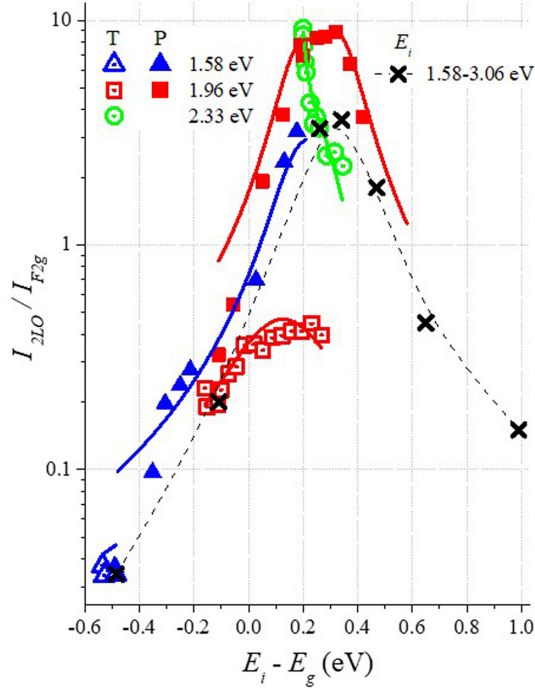


FIG. 8. The excitation energy, pressure and temperature dependent R ratio as a function of $\Delta = E_i - E_g$ and their fits according to Eqs. (3) and (4).

resonant intensity; as manifested in the projection on the Δ - R ratio plane, the span of Δ up to 30 GPa practically covers a significant fraction (~ 0.8 eV) of the full resonant profile. For the temperature dependent case the significant effect on the R ratio dependence, when E_i is slightly altered between the I_{in} and I_{out} “dominant regions,” is clearly demonstrated. In addition, increasing the temperature up to ~ 900 K covers a Δ window of ~ 0.45 eV which is $\sim 60\%$ of the window covered in the high pressures case. Hence, fully exploring the energy range of the temperature dependent resonant profile requires multiple measurements of sequential E_i shifts.

The R ratios as a function of $\Delta(T) = E_i - E_g(T)$ and $\Delta(P) = E_i - E_g(P)$ for the denoted E_i and their fits by employing Eqs. (3) and (4) and calculating $I_{in} + I_{out}$ are shown in Fig. 8 with empty and filled symbols, respectively. For comparison the ambient conditions $\Delta(E_i)$ in the range of

1.58–3.06 eV are shown with black cross symbols. Fitting the experimental data is done by employing the parameters used in the calculated profiles shown in Figs. 7(a) and 7(b).

The dominant role played by lifetime broadening effects in “suppressing” the resonant R ratio at high temperatures can be realized when noticing the decrease by a factor of ~ 20 in the intensity of the R ratios at $\Delta \approx 0.2$ eV ($\Delta \approx \delta$) for the measured point at 2.33 eV (77 K) relative to that of 1.96 eV (~ 750 K). In the absence of temperature-induced increase of the excited-state lifetime broadening, the R ratios of both measurements should have been about similar.

As a final note we emphasize that the most important outcome from presenting the fitted R ratio data in the form of Δ dependence is the demonstrated ability to jointly analyze, within a single framework, the excitation energy, pressure and temperature effects on the resonant Raman response.

IV. CONCLUSIONS

UO₂ exhibits excitation energy ($E_i = 1.58$ – 3.06 eV), temperature (77–873 K), and pressure (≤ 29 GPa) dependent Fröhlich interaction induced resonant multi-LO(Γ)-phonon Raman scattering. For the first LO(Γ) overtone, the incoming resonance of an optical transition positioned at $\delta \sim 0.19$ above the ~ 2.1 eV band gap and its respective outgoing resonance are successfully analyzed under a single framework. The energy of this transition is proposedly related to the Brillouin zone Γ point electronic density of states, positioned by recent DFT calculations to be slightly above the band gap.

The interplay between the temperature dependent simultaneous effects of tuning the band gap and the lifetime broadening of the excited electronic state is elucidated, and demonstrated to strongly depend on the excitation energy and its position with respect to the band gap.

ACKNOWLEDGMENTS

Dr. Leila Zeiri from the Ilse Katz Institute for Nanoscale Science and Technology in Ben-Gurion University, Dr. Iddo Pinkas from the chemical services of Weizmann institute, and Prof. Ariel Ismach from the Department of Materials Science in Tel-Aviv University are gratefully acknowledged for kindly assisting with multiwavelength analysis by enabling access to their Raman spectrometers. Dr. Genady Rafailov is also gratefully acknowledged for measuring the XRD and performing the analysis of the used UO₂ pellet.

- [1] J. Schoenes, *Phys. Rep.* **63**, 301 (1980).
- [2] J. Schoenes, *J. Chem. Soc., Faraday Trans. 2* **83**, 1205 (1987).
- [3] K. N. Kudin, G. E. Scuseria, and R. L. Martin, *Phys. Rev. Lett* **89**, 266402 (2002).
- [4] S. M. Gilbertson, T. Durakiewicz, G. L. Dakovski, Y. Li, J.-X. Zhu, S. D. Conradson, S. A. Trugman, and G. Rodriguez, *Phys. Rev. Lett.* **112**, 087402 (2014).
- [5] S. W. Yu, J. Tobin, J. C. Crowhurst, S. Sharma, J. K. Dewhurst, P. O. Velasco, W. L. Yang, and W. J. Siekhaus, *Phys. Rev. B* **83**, 165102 (2011).

- [6] T. Livneh and E. Sterer, *Phys. Rev. B* **73**, 085118 (2006).
- [7] In equilibrium, the population of the crystal field (CF) levels obeys the Boltzmann statistics and the intensity of the electronic Raman scattering from an initial level l after summation over all j atomic levels is proportional to $\exp(-E_l/kT) / \sum_j \exp(-E_j/kT)$. Since the ground state population decreases with increasing temperature the Stokes Raman scattering signal from the CF transition is expected to decrease in intensity. This is in contrast with the off-resonant intensity of a second-order phonon band with similar energy which is proportional to $(n(\omega_{LO}) + 1)^2$, $(n(\omega_p) = [\exp(\hbar\omega_p/kT) - 1]^{-1})$.

- The decrease in the intensity of the $\sim 1150\text{ cm}^{-1}$ band, found upon raising the temperature, led Schoenes [2] to its attribution to the $\Gamma_5-\Gamma_3$ electronic Raman CF transition.
- [8] H. X. Song, H. Y. Geng, and Q. Wu, *Phys. Rev. B* **85**, 064110 (2012).
- [9] P. Y. Yu and M. Cardona, *Fundamentals of Semiconductors* (Springer-Verlag, Berlin, 1999), p. 393.
- [10] R. Merlin, G. Güntherodt, R. Humphreys, M. Cardona, R. Suryanarayanan, and F. Holtzberg, *Phys. Rev. B* **17**, 4951 (1978).
- [11] K. Syassen, H. Winzen, H. G. Zimmer, and H. Tups, *Phys. Rev. B* **32**, 8246 (1985).
- [12] See Supplemental Material at <http://link.aps.org/supplemental/10.1103/PhysRevB.105.045115> for XRD of the UO_2 pellet, symmetry assignments, and second-order transitions in UO_2 ; ambient conditions Raman spectra at 1.58–3.06 eV; temperature dependence of the band gap extracted from previous absorption and reflectivity studies; effect of temperature dependent lifetime broadening on the position of incoming and outgoing resonances; and the fit of the broadening parameter from experimental results for E_i of 1.96 eV.
- [13] G. Leinders, T. Cardinaels, K. Binnemans, and M. Verwerft, *J. Nucl. Mater.* **459**, 135 (2015).
- [14] J. W. L. Pang, A. Chernatynskiy, B. C. Larson, W. J. L. Buyers, D. L. Abernathy, K. J. McClellan, and S. R. Phillpot, *Phys. Rev. B* **89**, 115132 (2014).
- [15] G. Dolling, R. A. Cowley, and A. D. B. Woods, *Can. J. Phys.* **43**, 1397 (1965).
- [16] W. Weber, K. Hass, and J. McBride, *Phys. Rev. B* **48**, 178 (1993).
- [17] M. S. Dresselhaus, G. Dresselhaus, and A. Jorio, *Group Theory: Application to the Physics of Condensed Matter* (Springer, Berlin, 2008) p. 209.
- [18] G. Turrell, *Infrared and Raman Spectra of Crystals* (Academic, New York, 1972), p. 297.
- [19] E. B. Wilson, Jr., J. C. Decius, and P. C. Cross, *Molecular Vibrations: The Theory of Infrared and Raman Vibrational Spectra* (Dover, New York, 1955), p. 331.
- [20] P. K. Morgan, T. A. Prusnick, M. A. Velez, K. Rickert, D. B. Turner, and J. M. Mann, *J. Raman Spectrosc.* **52**, 1901 (2021).
- [21] T. R. Griffiths and H. V. St. A. Hubbard, *J. Nucl. Mater.* **185**, 243 (1991).
- [22] P. Ruello, R. D. Becker, K. Ullrich, L. Desgranges, C. Petot, and G. Petot-Ervas, *J. Nucl. Mater.* **328**, 46 (2004).
- [23] J. C. Crowhurst, J. R. Jeffries, D. Åberg, J. M. Zaug, Z. R. Dai, W. J. Siekhaus, N. E. Teslich, K. S. Holliday, K. B. Knight, A. J. Nelson, and I. D. Hutcheon, *J. Phys.: Condens. Matter* **27**, 265401 (2015).
- [24] J. M. Elorrieta, L. J. Bonales, and V. G. Baonza, *J. Nucl. Mater.* **503**, 191 (2018).
- [25] O. A. Maslova, X. Iltis, L. Desgranges, M. R. Ammar, C. Genevois, E. de Bilbao, A. Canizares, S. A. Barannikova, I. N. Leontyev, and P. Simon, *Mater. Charact.* **147**, 280 (2019).
- [26] L. Desgranges, G. Baldinozzi, P. Simon, G. Guimbretière, and A. Canizares, *J. Raman Spectrosc.* **43**, 455 (2012).
- [27] Q. Zhang, J. Zhang, M. I. B. Utama, B. Peng, M. de la Mata, J. Arbiol, and Q. Xiong, *Phys. Rev. B* **85**, 085418 (2012).
- [28] G. Amoretti, A. Blaise, R. Caciuffo, J. M. Fournier, M. T. Hutchings, R. Osborn, and A. D. Taylor, *Phys. Rev. B* **40**, 1856 (1989).
- [29] G. H. Lander, M. Sundermann, R. Springell, A. C. Walters, A. Nag, M. Garcia-Fernandez, K. J. Zhou, G. van der Laan, and R. Caciuffo, *J. Phys.: Condens. Matter* **33**, 06LT01 (2021).
- [30] C. A. Morrison and R. P. Leavitt, Spectroscopic properties of triply ionized lanthanides in transparent host crystals, in *Handbook on the Physics and Chemistry of Rare Earths*, Vol. 5, edited by K. A. Gschneidner, Jr. and L. Eyring (North-Holland, Amsterdam, 1982), p. 461.
- [31] A. Sethi, J. E. Slimak, T. Kolodiazny, and S. L. Cooper, *Phys. Rev. Lett* **122**, 177601 (2019).
- [32] T. A. Olds, S. E. Karcher, K. W. Kriegsman, X. Guo, and J. S. McCloy, *J. Nucl. Mater.* **530**, 151959 (2020).
- [33] R. Martin, *Phys. Rev. B* **10**, 2620 (1974).
- [34] M. Cardona, in *Light Scattering in Solids II*, edited by M. Cardona and G. Güntherodt, *Topics in Applied Physics* Vol. 50 (Springer-Verlag, Berlin, 1982), p. 19.
- [35] L. Huang, Y. Wang, and P. Werner, *EPL* **119**, 57007 (2017).
- [36] The attribution of a state to an exciton, which is formed by $\text{U}^{3+}-\text{U}^{5+}$ excitations that remain localized on $5f$ sites [4] cannot be ruled out but is considered to be rather unlikely, as there is no evidence of their localization within a particular energy range of the conduction band.
- [37] G. Guimbretière, A. Canizarès, N. Raimboux, J. Joseph, P. Desgardin, L. Desgranges, C. Jegou, and P. Simon, *J. Raman Spectrosc.* **46**, 418 (2015).
- [38] P. Lautenschlager, M. Garriga, S. Logothetidis, and M. Cardona, *Phys. Rev. B* **35**, 9174 (1987).
- [39] Models that have been used to elucidate the Fröhlich interaction induced resonant Raman scattering by $\text{LO}(\Gamma)$ phonon and its overtones are commonly categorized into two types: those based on Franck-Condon mechanisms in molecular spectroscopy such as employed for YbS [10] and those based on some form of perturbation calculation. The latter is possibly within the “cascade model,” where electrons cascade down the conduction band as they emit $\text{LO}(\Gamma)$ phonons [34]. This model commonly requires the resonance process to be exciton-intermediated, which, as stated above, is not unequivocally supported by our knowledge. Here, acceptable correspondence with the experimental results was only achieved by a scheme of two “separately counted” weighted contributions of $I_{\text{in}} + I_{\text{out}}$ terms. In the Franck-Condon formalism of configuration of interaction analysis [10] the term included in the model correlates with our I_{out} only. The perturbative approach with “coupled” resonances, which are introduced as vanishing terms in a denominator (squared), could not lead to an adequate correspondence with the experimental results.
- [40] R. Rentz and H. J. Schultz, *J. Lumin.* **24-25**, 221 (1981).